

Vector-controlled Y-connected three-phase induction motor drives: small-signal stability study during IGBT short-circuit fault

Maryam Naghavi¹, Mahmood Ghanbari¹, Reza Ebrahimi¹, Mohammad Jannati¹, Tole Sutikno^{2,3}

¹Department of Electrical Engineering, Gorgan Branch, Islamic Azad University, Gorgan, Iran

²Department of Electrical Engineering, Faculty of Industrial Technology, Universitas Ahmad Dahlan (UAD), Yogyakarta, Indonesia

³Embedded System and Power Electronic Research Group (ESPERG), Yogyakarta, Indonesia

Article Info

Article history:

Received Jan 20, 2023

Revised Feb 21, 2023

Accepted Mar 8, 2023

Keywords:

IGBT short-circuit fault

Induction motor drive

IRFOC

Small-signal stability analysis

Y-connected motor

ABSTRACT

The stability analysis is one of the most important elements to describe the performance of AC drive systems under both dynamic and steady-state operating circumstances. This is particularly essential because electric motors operate over a wide range of speeds and utilize complex control systems such as field-oriented control (FOC). This study establishes a small-signal stability analysis (SSSA) in a 1-horsepower vector-controlled Y-connected three-phase induction motor (YCTPIM) drive during an insulated gate bipolar transistor short-circuits failure (IGBT-SCF). In the beginning, a vector control system that is based on the indirect rotor FOC (IRFOC) method is described for post-fault functioning of the YCTPIM while the IGBT-SCF is taking place. After that, a small-signal model of the system that has been provided is explored. This model is based on a voltage-current model, and it is constructed by linearizing the non-linear dynamic equations of the system. During IGBT-SCF, an IRFOC strategy as well as SSSA operations are carried out on the 1-HP, 380 V, and YCTPIM. In this research, both analytical and simulation-based methodologies are applied.

This is an open access article under the [CC BY-SA](https://creativecommons.org/licenses/by-sa/4.0/) license.



Corresponding Author:

Mahmood Ghanbari

Department of Electrical Engineering, Gorgan Branch, Islamic Azad University

Gorgan, Iran

Email: ghanbari@gorganiau.ac.ir

NOMENCLATURE

Superscripts s, e	: Stationary and rotating reference frames
Superscripts f, h	: Faulty and healthy conditions
Subscript o	: Steady-state value
p	: Differential operator
$i_{ds}, i_{qs}, i_{dr}, i_{qr}, v_{ds}, v_{qs}, v_{dr}, v_{qr}$: Stator and rotor currents and voltages
v_1, v_2, v_3, v_4	: Stator forward and backward voltages
τ_e, τ_l	: Electromagnetic torque and load torque
ψ_{dr}, ψ_{qr}	: Rotor fluxes
$ \psi_r , \xi_e$: Rotor flux amplitude and angle
L_{ds}, L_{qs}, L_d, L_q	: Stator self and mutual inductances
L_r	: Rotor self-inductance
L_{ms}	: Magnetizing inductance

R_s, R_r	: Stator and rotor resistances
Ω_r, Ω_e	: Rotor speed and angular speed
n_p	: Number of pole pairs
J, F	: Moment of inertia and viscous friction coefficient
x, u, y	: State, input, and output matrices
f, h	: Nonlinear function of the states and linear function of the outputs
A, B	: System matrix and input matrix
$[k_{si}^{ef}], [k_{sv}^{ef}], [k_s^{eh}]$: Balanced and unbalanced transformation matrices during faulty and healthy conditions
$[k_s^f], [k_s^h]$: 2 to 2 transformation matrices during faulty and healthy conditions

1. INTRODUCTION

In low, medium, and high-power industrial applications, three-phase induction motor (TPIM) drives are the most often utilized AC drives. Its key advantages are its low cost and size, toughness, and roughness, as well as the absence of a brush and commutator [1]. Many industrial TPIM drives are intended to work well even when problems arise. Examples of such uses include electric vehicles, military equipment, and medical equipment. TPIM drives can function even when a slight malfunction occurs thanks to fault-tolerant control (FTC) techniques [2]–[5].

Different faults can occur in AC drives. Approximately 38% of faults in AC drive systems are related to power device faults [6]. Most AC drives use an insulated gate bipolar transistor (IGBT) as the power device. Although IGBTs are rugged, they suffer faults because of electrical, mechanical, and thermal stress. IGBT faults can be classified as open-circuit faults (OCFs) and short-circuit faults (SCFs). Insulated gate bipolar transistor short-circuit fault (IGBT-SCF) is one of the most common faults in AC drive systems. This type of fault significantly degrades the performance of the drive system and may lead to catastrophic failures [7].

Pre-fault operation, fault diagnosis, and post-fault operation are the three components that make up fault tolerance control in TPIM drives during IGBT-SCF. The post-fault operation of TPIM drives during IGBT-SCF involves two primary trends: the architecture of the power inverter and the post-fault control method. In order to run Y-connected three-phase motors following IGBT-SCF, several different power inverter topologies have been developed. These architectures are based on some hardware redundancy. If the Y-connected three-phase motor's neutral point (NP) can be accessed, a reconfiguration scheme can be presented by connecting the NP to a fourth leg of the inverter leg [8] or by connecting the NP to the middle point of the DC bank [9]. Both of these connections are possible if the NP is available. If the Y-connected three-phase motor's neutral point (NP) cannot be reached, a reconfiguration scheme can be presented by connecting the motor terminal of the faulted inverter leg to a fourth inverter leg [10] or by connecting the motor terminal of the faulted inverter leg to the middle point of the DC bank [11]. Both of these options are available in the event that the NP cannot be reached. The inverter architecture that was examined for this research for post-fault operation of the Y-connected TPIM (YCTPIM) during IGBT-SCF is based on [9], and it is depicted in Figure 1.

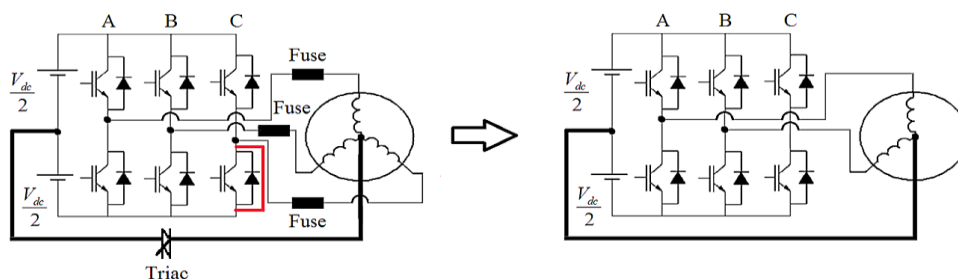


Figure 1. Investigated inverter architecture in this research for post-fault operation of the YCTPIM during IGBT-SCF

As can be observed in Figure 1, when the inverter topology that has been developed in this study is utilized, the motor operates as a two-phase motor. For the purpose of driving the two-phase motor, a number of different control strategies based on scalar control methods [12] and vector control methods [13]–[18] have been developed. Scalar control schemes are typically straightforward, making them suitable for implementation in real time because of their ease of use. Nevertheless, high-performance control of AC

drives is not an appropriate application for these strategies. In this scenario, field-oriented control (FOC) or vector control are the tactics that are going to be most effective. It has been suggested to operate the two-phase motor using a variety of control strategies, some of which are based on indirect vector control techniques [13]–[17] and others on direct vector control techniques [18]. Due to the utilization of two different vector control systems, the procedure that is suggested in [13] is quite complicated and necessitates a high sampling frequency. The vector control method described in requires different strategies to be implemented depending on the type of fault that has occurred. The control techniques described in [15]–[18] are based on two imbalanced transformation matrices for the voltage and current components of the stator. The difficulty of the backward voltage computation is a drawback of these methods.

It is required to evaluate the control qualities of the motor drive system over a broad range of speeds in order to execute complex control techniques like FOC. These strategies need a great deal of planning and preparation. The operation has a significant impact on the manner in which a motor drive system works. Over the course of the last few decades, numerous research articles on the subject of the stability analysis of TPIM drive systems have been published [19]–[23]. In [19], the instability of a TPIM that was being driven by a variable-frequency drive was shown. This presentation took into account the effect of TPIM parameters, but it ignored the effect of harmonics. The stability analysis of a rectifier-inverter TPIM drive has been carried out using the Nyquist stability criterion. This analysis neglects voltage harmonics. The analysis can be found in [20]. In [21], the authors show the stability of current-controlled TPIM drives achieved through the application of the transfer function technique. Islam *et al.* [22] present a basic small-signal stability analysis (SSSA) of a vector-controlled TPIM drive based on a voltage-flux-linkage model. This analysis was carried out in order to determine whether or not the drive is stable under small signals. It has been demonstrated in [23] how to calculate the SSSA of an open-loop TPIM drive while taking into account the effect of the inverter's dead time. As was said before, stability studies in TPIM drive systems have been extensively covered in the aforementioned body of research. However, research activities in this field have never veered their attention away from TPIM drives that are in good health.

This work discusses the SSSA of vector-controlled YCTPIM drives while operating in an IGBT-SCF environment. In order to achieve this goal, the voltage-current model is constructed from the d-q dynamic model, which is then stated in the rotating reference frame. The d-q motor equations are linearized around a steady-state operating point in order to get small signal equations. This is done so that the stability of the motor can be evaluated. Following the linearization process, code written in MATLAB is used to analyze the problematic YCTPIM drive's stability. The most important thing that this research has contributed is the creation of a linearized voltage-current model of the flawed YCTPIM drive and the use of this model to stability investigations.

2. IRFOC OF THE YCTPIM DRIVE DURING IGBT-SCF

FOC strategies are widely used in many modern high-performance AC drive applications, especially TPIM electric drives, due to their high accuracy. When compared to the traditional direct torque control (DTC) strategy, TPIM drives achieve high performance with a constant switching frequency and low torque ripples [24], [25]. In order to control the two-phase motor using the FOC strategy, two unbalanced transformation matrices have been presented and used in [15]. These matrices are (1) and (2).

$$\begin{bmatrix} i_{ds}^e \\ i_{qs}^e \end{bmatrix} = [k_{si}^{ef}] \begin{bmatrix} i_{ds}^s \\ i_{qs}^s \end{bmatrix} = \begin{bmatrix} \sqrt{3} \cos \xi_e & \sin \xi_e \\ -\sqrt{3} \sin \xi_e & \cos \xi_e \end{bmatrix} \begin{bmatrix} i_{ds}^s \\ i_{qs}^s \end{bmatrix} \quad (1)$$

$$\begin{bmatrix} v_{ds}^e \\ v_{qs}^e \end{bmatrix} = [k_{sv}^{ef}] \begin{bmatrix} v_{ds}^s \\ v_{qs}^s \end{bmatrix} = \begin{bmatrix} \frac{\sqrt{3}}{3} \cos \xi_e & \sin \xi_e \\ -\frac{\sqrt{3}}{3} \sin \xi_e & \cos \xi_e \end{bmatrix} \begin{bmatrix} v_{ds}^s \\ v_{qs}^s \end{bmatrix} \quad (2)$$

Using (1), (2), and assuming $|\psi_{dr}^e| = |\psi_r|$ and $|\psi_{qr}^e| = 0$, the RFOC equations of the two-phase motor can be achieved as (3)-(5).

$$|\psi_r| = L_q i_{ds}^e - \frac{L_r}{R_r} p |\psi_r| \quad (3)$$

$$\tau_e = \frac{n_p L_q}{L_r} |\psi_r| i_{qs}^e \quad (4)$$

$$\Omega_e = \Omega_r + \frac{R_r L_q}{L_r} \frac{1}{|\psi_r|} i_{qs}^e = \Omega_r + \frac{R_r}{L_r} \frac{i_{qs}^e}{i_{ds}^e} \quad (5)$$

Where:

$$L_q = \frac{\sqrt{3}}{2} L_{ms} \tag{6}$$

based on (1)-(6), the IRFOC scheme for post-fault control of YCTPIM drives during IGBT-SCF can be shown as Figure 2 [16].

$$[k_s^f] = \frac{\sqrt{2}}{2} \begin{bmatrix} 1 & -1 \\ 1 & 1 \end{bmatrix} \tag{7}$$

In order to compare the presented IRFOC scheme is shown in Figure 2 with the conventional controller, the block diagram of the conventional IRFOC scheme is shown in Figure 3 [15]:

$$L = \frac{3}{2} L_{ms} \tag{8}$$

$$[k_s^h] = \sqrt{\frac{2}{3}} \begin{bmatrix} 1 & -0.5 \\ 0 & \frac{\sqrt{3}}{2} \end{bmatrix} \tag{9}$$

$$[k_s^{eh}] = \begin{bmatrix} \cos \xi_e & \sin \xi_e \\ -\sin \xi_e & \cos \xi_e \end{bmatrix} \tag{10}$$

It is worth noting that the proposed IRFOC method of Figure 2 is based on a current control strategy. This control system unlike [15] has simple structure due to avoiding of calculating of the backward stator voltages.

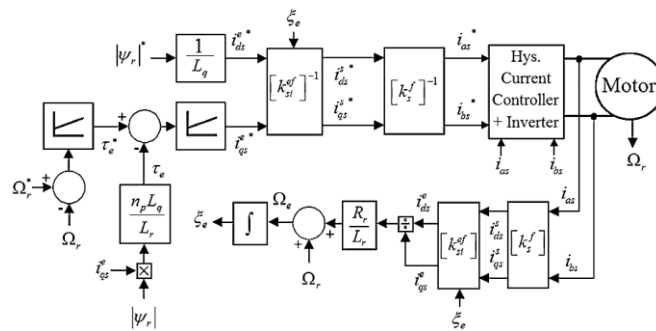


Figure 2. IRFOC scheme for post-fault control of YCTPIM drives during IGBT-SCF

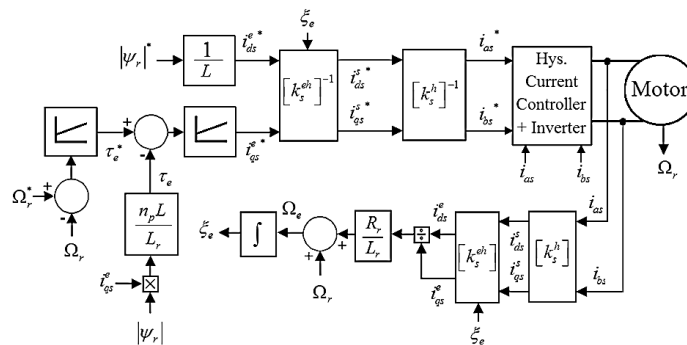


Figure 3. Conventional IRFOC scheme

3. SMALL-SIGNAL STABILITY ANALYSIS (SSSA)

Stability analysis is a significant qualitative characteristic of electrical machine drive systems. This section discusses the SSSA of the presented system using root locus contours. At first, the dynamic model of the system is presented by nonlinear differential equations. Then, this model is linearized, and the corresponding state space form is derived. It is worth noting that the effects of inverter dead time, harmonics, motor parameter variations, the particular value of the load, etc. are not considered in this analysis. Using (1) and (2), the voltage and torque equations of the two-phase motor can be written as (11)–(17) [15].

$$v_1 = R_s i_{ds}^e + L_{qs} p i_{ds}^e - \Omega_e L_{qs} i_{qs}^e + L_q p i_{dr}^e - \Omega_e L_q i_{qr}^e \tag{11}$$

$$v_2 = -\frac{2}{3} R_s i_{ds}^{-e} + \left(\frac{1}{3} L_{ds} - L_{qs}\right) p i_{ds}^{-e} - \Omega_e \left(\frac{1}{3} L_{ds} - L_{qs}\right) i_{qs}^{-e} \tag{12}$$

$$v_3 = R_s i_{qs}^e + L_{qs} p i_{qs}^e + \Omega_e L_{qs} i_{ds}^e + L_q p i_{qr}^e + \Omega_e L_q i_{dr}^e \tag{13}$$

$$v_4 = -\frac{2}{3} R_s i_{qs}^{-e} + \left(\frac{1}{3} L_{ds} - L_{qs}\right) p i_{qs}^{-e} + \Omega_e \left(\frac{1}{3} L_{ds} - L_{qs}\right) i_{ds}^{-e} \tag{14}$$

$$v_{dr}^e = L_q p i_{ds}^e - (\Omega_e - \Omega_r) L_q i_{qs}^e + R_r i_{dr}^e + L_r p i_{dr}^e - (\Omega_e - \Omega_r) L_r i_{qr}^e \tag{15}$$

$$v_{qr}^e = L_q p i_{qs}^e + (\Omega_e - \Omega_r) L_q i_{ds}^e + R_r i_{qr}^e + L_r p i_{qr}^e + (\Omega_e - \Omega_r) L_r i_{dr}^e \tag{16}$$

$$n_p \left(\frac{n_p L_q}{L_r} |\psi_r| i_{qs}^e - \tau_l \right) = J p \Omega_r + F \Omega_r \tag{17}$$

Where:

$$\begin{bmatrix} i_{ds}^{-e} \\ i_{qs}^{-e} \end{bmatrix} = \begin{bmatrix} \cos^2 \xi_e & -\frac{1}{2} \sin 2 \xi_e \\ -\frac{1}{2} \sin 2 \xi_e & \sin^2 \xi_e \end{bmatrix} \begin{bmatrix} i_{ds}^e \\ i_{qs}^e \end{bmatrix} \tag{18}$$

The dynamic model of the system can be expressed by the following overall nonlinear representation:

$$\begin{cases} \dot{p}x = f(x, u) \\ y = h(x) \end{cases} \tag{19}$$

where, the states, the inputs, and the outputs are:

$$x = [x_1 \ x_2 \ x_3 \ x_4 \ x_5 \ x_6 \ x_7]^T = [i_{ds}^e \ i_{qs}^e \ i_{ds}^{-e} \ i_{qs}^{-e} \ i_{dr}^e \ i_{qr}^e \ \Omega_r]^T \tag{20}$$

$$u = [u_1 \ u_2 \ u_3 \ u_4 \ u_5 \ u_6 \ u_7 \ u_8]^T = [v_1 \ v_2 \ v_3 \ v_4 \ v_{dr}^e \ v_{qr}^e \ \Omega_e \ \tau_l]^T \tag{21}$$

$$y = [y_1 \ y_2 \ y_3 \ y_4]^T = [i_{ds}^e \ i_{qs}^e \ i_{ds}^{-e} \ i_{qs}^{-e}]^T \tag{22}$$

based on (11)-(22), the nonlinearity f and the linearity h are given by (23) and (24), respectively.

$$\begin{bmatrix} p x_1 \\ p x_2 \\ p x_3 \\ p x_4 \\ p x_5 \\ p x_6 \\ p x_7 \end{bmatrix} = f(x, u) = \begin{bmatrix} \frac{1}{L_{qs} \left(1 - \frac{L_q^2}{L_r L_{qs}}\right)} \left(u_1 - R_s x_1 + L_{qs} u_7 x_2 - \frac{L_q^2}{L_r} u_7 x_2 + \frac{L_q^2}{L_r} x_2 x_7 + \frac{L_q R_r}{L_r} x_5 + L_q x_6 x_7 \right) \\ \frac{1}{L_{qs} \left(1 - \frac{L_q^2}{L_r L_{qs}}\right)} \left(u_3 - R_s x_2 - L_{qs} u_7 x_1 + \frac{L_q^2}{L_r} u_7 x_1 - \frac{L_q^2}{L_r} x_1 x_7 + \frac{L_q R_r}{L_r} x_6 - L_q x_5 x_7 \right) \\ \frac{1}{\frac{1}{3} L_{ds} - L_{qs}} \left(u_2 + \frac{2}{3} R_s x_3 + \left(\frac{1}{3} L_{ds} - L_{qs}\right) u_7 x_4 \right) \\ \frac{1}{\frac{1}{3} L_{ds} - L_{qs}} \left(u_4 + \frac{2}{3} R_s x_4 - \left(\frac{1}{3} L_{ds} - L_{qs}\right) u_7 x_3 \right) \\ \frac{1}{L_q \left(1 - \frac{L_r L_{qs}}{L_q^2}\right)} \left(u_1 - R_s x_1 + L_{qs} x_2 x_7 + \frac{L_{qs} R_r}{L_q} x_5 - \frac{L_{qs} L_r}{L_q} u_7 x_6 + \frac{L_{qs} L_r}{L_q} x_6 x_7 + L_q u_7 x_6 \right) \\ \frac{1}{L_q \left(1 - \frac{L_r L_{qs}}{L_q^2}\right)} \left(u_3 - R_s x_2 - L_{qs} x_1 x_7 + \frac{L_{qs} R_r}{L_q} x_6 + \frac{L_{qs} L_r}{L_q} u_7 x_5 - \frac{L_{qs} L_r}{L_q} x_5 x_7 - L_q u_7 x_5 \right) \\ \frac{1}{J} \left(-F x_7 + n_p \left(\frac{n_p L_q |\psi_r|}{L_r} x_2 - u_8 \right) \right) \end{bmatrix} \tag{23}$$

$$h = \begin{bmatrix} x_1 \\ x_2 \\ x_3 \\ x_4 \end{bmatrix} \tag{24}$$

As can be seen from (23), the presented system is a non-linear system, and a small signal model is derived to achieve the stability analysis of the system. At a steady-state operating condition, the corresponding perturbations in the state and input variables can be expressed by $X = [X_1 \ X_2 \ X_3 \ X_4 \ X_5 \ X_6 \ X_7]^T =$

$[\delta i_{ds}^e \ \delta i_{qs}^e \ \delta i_{ds}^{-e} \ \delta i_{qs}^{-e} \ \delta i_{dr}^e \ \delta i_{qr}^e \ \delta \Omega_r]^T$ and $U = [U_1 \ U_2 \ U_3 \ U_4 \ U_5 \ U_6 \ U_7 \ U_8]^T = [\delta v_1 \ \delta v_2 \ \delta v_3 \ \delta v_4 \ \delta v_{dr}^e \ \delta v_{qr}^e \ \delta \Omega_e \ \delta \tau_l]^T$, respectively. In addition, the motor components after perturbation can be written as (25).

$$\begin{aligned} v_1 &= v_{10} + \delta v_1, \quad v_2 = v_{20} + \delta v_2, \quad v_3 = v_{30} + \delta v_3, \quad v_4 = v_{40} + \delta v_4 \\ v_{dr}^e &= v_{dro}^e + \delta v_{dr}^e, \quad v_{qr}^e = v_{qro}^e + \delta v_{qr}^e, \quad i_{ds}^e = i_{dso}^e + \delta i_{ds}^e, \quad i_{qs}^e = i_{qso}^e + \delta i_{qs}^e \\ i_{dr}^e &= i_{dro}^e + \delta i_{dr}^e, \quad i_{qr}^e = i_{qro}^e + \delta i_{qr}^e, \quad i_{ds}^{-e} = i_{dso}^{-e} + \delta i_{ds}^{-e}, \quad i_{qs}^{-e} = i_{qso}^{-e} + \delta i_{qs}^{-e} \\ \tau_e &= \tau_{e0} + \delta \tau_e, \quad \tau_l = \tau_{l0} + \delta \tau_l, \quad \Omega_e = \Omega_{e0} + \delta \Omega_e, \quad \Omega_r = \Omega_{r0} + \delta \Omega_r \end{aligned} \tag{25}$$

Using (25), the stator and rotor d-q voltage equations and the electromagnetic torque equation can be written as (26)-(32).

$$\delta v_1 = R_s \delta i_{ds}^e + L_{qs} p \delta i_{ds}^e - L_{qs} \Omega_{e0} \delta i_{qs}^e + L_q p \delta i_{dr}^e - L_q \Omega_{e0} \delta i_{qr}^e - (L_{qs} i_{qso}^e + L_q i_{qro}^e) \delta \Omega_e \tag{26}$$

$$\delta v_2 = -\frac{2}{3} R_s \delta i_{ds}^{-e} + \left(\frac{1}{3} L_{ds} - L_{qs}\right) p \delta i_{ds}^{-e} - \left(\frac{1}{3} L_{ds} - L_{qs}\right) \Omega_{e0} \delta i_{qs}^{-e} - \left(\frac{1}{3} L_{ds} - L_{qs}\right) i_{qso}^{-e} \delta \Omega_e \tag{27}$$

$$\delta v_3 = R_s \delta i_{qs}^e + L_{qs} p \delta i_{qs}^e + L_{qs} \Omega_{e0} \delta i_{ds}^e + L_q p \delta i_{qr}^e + L_q \Omega_{e0} \delta i_{dr}^e + (L_{qs} i_{dso}^e + L_q i_{dro}^e) \delta \Omega_e \tag{28}$$

$$\delta v_4 = -\frac{2}{3} R_s \delta i_{qs}^{-e} + \left(\frac{1}{3} L_{ds} - L_{qs}\right) p \delta i_{qs}^{-e} + \left(\frac{1}{3} L_{ds} - L_{qs}\right) \Omega_{e0} \delta i_{ds}^{-e} + \left(\frac{1}{3} L_{ds} - L_{qs}\right) i_{dso}^{-e} \delta \Omega_e \tag{29}$$

$$\begin{aligned} \delta v_{dr}^e &= L_q p \delta i_{ds}^e - \Omega_{s0} L_q \delta i_{qs}^e + R_r \delta i_{dr}^e + \\ &L_r p \delta i_{dr}^e - \Omega_{s0} L_r \delta i_{qr}^e + (L_q i_{qso}^e + L_r i_{qro}^e) (\delta \Omega_r - \delta \Omega_e) \end{aligned} \tag{30}$$

$$\begin{aligned} \delta v_{qr}^e &= L_q p \delta i_{qs}^e + \Omega_{s0} L_q \delta i_{ds}^e + R_r \delta i_{qr}^e + \\ &L_r p \delta i_{qr}^e + \Omega_{s0} L_r \delta i_{dr}^e - (L_q i_{dso}^e + L_r i_{dro}^e) (\delta \Omega_r - \delta \Omega_e) \end{aligned} \tag{31}$$

$$n_p^2 \left(L_q i_{qso}^e \delta i_{dr}^e + L_q i_{dro}^e \delta i_{qs}^e - L_q i_{dso}^e \delta i_{qr}^e - L_q i_{qro}^e \delta i_{ds}^e - \frac{\delta \tau_l}{n_p} \right) = J p \Omega_r + F \delta \Omega_r \tag{32}$$

Where:

$$\Omega_{s0} = \Omega_{e0} - \Omega_{r0} \tag{33}$$

in (26)-(33) can be arranged as (34).

$$\begin{aligned} \begin{bmatrix} pX_1 \\ pX_2 \\ pX_3 \\ pX_4 \\ pX_5 \\ pX_6 \\ pX_7 \end{bmatrix} &= \begin{bmatrix} -\frac{L_r R_s}{L_{qs} L_r - L_q^2} & \frac{L_{qs} L_r \Omega_{e0}}{L_{qs} L_r - L_q^2} - \frac{L_q^2 \Omega_{s0}}{L_{qs} L_r - L_q^2} & 0 & 0 & \frac{L_q R_r}{L_{qs} L_r - L_q^2} & \frac{L_r L_q \Omega_{e0}}{L_{qs} L_r - L_q^2} - \frac{L_r L_q \Omega_{s0}}{L_{qs} L_r - L_q^2} & -\frac{L_q (-L_r i_{qro} - L_q i_{qso})}{L_{qs} L_r - L_q^2} \\ -\frac{L_{qs} L_r \Omega_{e0}}{L_{qs} L_r - L_q^2} + \frac{L_q^2 \Omega_{s0}}{L_{qs} L_r - L_q^2} & -\frac{L_r R_s}{L_{qs} L_r - L_q^2} & 0 & 0 & -\frac{L_r L_q \Omega_{e0}}{L_{qs} L_r - L_q^2} + \frac{L_r L_q \Omega_{s0}}{L_{qs} L_r - L_q^2} & \frac{L_q R_r}{L_{qs} L_r - L_q^2} & -\frac{L_q (L_r i_{dro} + L_q i_{dso})}{L_{qs} L_r - L_q^2} \\ 0 & 0 & \frac{2R_s}{L_{ds} - 3L_{qs}} & \Omega_{e0} & 0 & 0 & 0 \\ 0 & 0 & -\Omega_{e0} & \frac{2R_s}{L_{ds} - 3L_{qs}} & 0 & 0 & 0 \\ \frac{L_q R_s}{L_{qs} L_r - L_q^2} & -\frac{L_{qs} L_q \Omega_{e0}}{L_{qs} L_r - L_q^2} + \frac{L_{qs} L_q \Omega_{s0}}{L_{qs} L_r - L_q^2} & 0 & 0 & -\frac{L_{qs} R_s}{L_{qs} L_r - L_q^2} & -\frac{L_q^2 \Omega_{e0}}{L_{qs} L_r - L_q^2} + \frac{L_{qs} L_r \Omega_{s0}}{L_{qs} L_r - L_q^2} & -\frac{L_{qs} (-L_r i_{qro} - L_q i_{qso})}{L_{qs} L_r - L_q^2} \\ \frac{L_{qs} L_q \Omega_{e0}}{L_{qs} L_r - L_q^2} - \frac{L_{qs} L_q \Omega_{s0}}{L_{qs} L_r - L_q^2} & \frac{L_{qs} R_s}{L_{qs} L_r - L_q^2} & 0 & 0 & \frac{L_q^2 \Omega_{e0}}{L_{qs} L_r - L_q^2} - \frac{L_{qs} L_r \Omega_{s0}}{L_{qs} L_r - L_q^2} & -\frac{L_{qs} R_s}{L_{qs} L_r - L_q^2} & \frac{L_{qs} (L_r i_{dro} + L_q i_{dso})}{L_{qs} L_r - L_q^2} \\ -\frac{L_q^2 \Omega_{e0} n_p^2}{J} & \frac{L_q i_{dro} n_p^2}{J} & 0 & 0 & \frac{L_q i_{qso} n_p^2}{J} & -\frac{L_q i_{dso} n_p^2}{J} & -\frac{F}{J} \end{bmatrix} \\ + \begin{bmatrix} \frac{L_r}{L_{qs} L_r - L_q^2} & 0 & 0 & 0 & -\frac{L_q}{L_{qs} L_r - L_q^2} & 0 & \frac{L_r (L_{qs} i_{qso} + L_q i_{qro})}{L_{qs} L_r - L_q^2} - \frac{L_q (L_r i_{qro} + L_q i_{qso})}{L_{qs} L_r - L_q^2} & 0 \\ 0 & 0 & \frac{L_r}{L_{qs} L_r - L_q^2} & 0 & 0 & -\frac{L_q}{L_{qs} L_r - L_q^2} & \frac{L_r (-L_{qs} i_{dso} - L_q i_{dro})}{L_{qs} L_r - L_q^2} - \frac{L_q (L_r i_{dro} - L_q i_{dso})}{L_{qs} L_r - L_q^2} & 0 \\ 0 & \frac{1}{\frac{2}{3} L_{ds} - L_{qs}} & 0 & 0 & 0 & 0 & i_{qso}^{-e} & 0 \\ 0 & 0 & 0 & \frac{1}{\frac{2}{3} L_{ds} - L_{qs}} & 0 & 0 & -i_{dso}^{-e} & 0 \\ -\frac{L_q}{L_{qs} L_r - L_q^2} & 0 & 0 & 0 & \frac{L_{qs}}{L_{qs} L_r - L_q^2} & 0 & -\frac{L_q (L_{qs} i_{qso} + L_q i_{qro})}{L_{qs} L_r - L_q^2} + \frac{L_{qs} (L_r i_{qro} + L_q i_{qso})}{L_{qs} L_r - L_q^2} & 0 \\ 0 & 0 & -\frac{L_q}{L_{qs} L_r - L_q^2} & 0 & 0 & \frac{L_{qs}}{L_{qs} L_r - L_q^2} & \frac{L_q (-L_{qs} i_{dso} - L_q i_{dro})}{L_{qs} L_r - L_q^2} + \frac{L_{qs} (-L_r i_{dro} - L_q i_{dso})}{L_{qs} L_r - L_q^2} & 0 \\ 0 & 0 & 0 & 0 & 0 & 0 & 0 & -\frac{n_p^2}{J} \end{bmatrix} \begin{bmatrix} U_1 \\ U_2 \\ U_3 \\ U_4 \\ U_5 \\ U_6 \\ U_7 \\ U_8 \end{bmatrix} \end{aligned} \tag{34}$$

Now, the perturbed system state equations are achieved after linearization and are shown in the typical form as (35).

$$pX = AX + BU \tag{35}$$

4. SIMULATION RESULTS

In this section, two simulations are carried out to investigate the performance of the system. Simulations are performed using MATLAB code. The parameters of the YCTPIM are listed in Table 1. In the first simulation, a comparison study between the proposed IRFOC method and the conventional IRFOC method for the YCTPIM drive during IGBT-SCF has been performed. Based on Figure 2, Figure 4(a) depicts the simulation results of the proposed IRFOC method. Figure 4(b) also depicts the simulation results of the conventional IRFOC method based on Figure 3. For a fair comparison in both simulations of Figure 4, the NP of the YCTPIM is connected to the middle point of the DC bank. The simulation results in Figure 4 are all obtained for the IGBT-SCF in leg "C." In Figure 4, the reference rotor speed decreases from 150 rad/s to 90 rad/s, and the reference rotor flux is 1 wb. The rotor flux, torque, stator line currents, speed, and zoom of speed signals are shown in Figure 4. Figure 4 shows that you can cover their references by using both controllers, speed and flux. Based on Figure 4, using both strategies, the rotor flux and speed are always stable during the decelerating process. However, according to this figure, using the proposed IRFOC method results in lower rotor flux, torque, and speed ripples compared to the conventional IRFOC method. As shown from the stator line currents, using the controller presented in this paper, the two-phase motor currents after the IGBT-SCF are balanced compared to the conventional controller.

Table 1. Parameters of the YCTPIM

Frequency (Hz)	$R_s(\Omega)$	$R_r(\Omega)$	$L_s = L_r(H)$	$L_{ms}(H)$	$J(kg.m^2)$
50	10.44	14.64	0.613	0.398 H	0.016

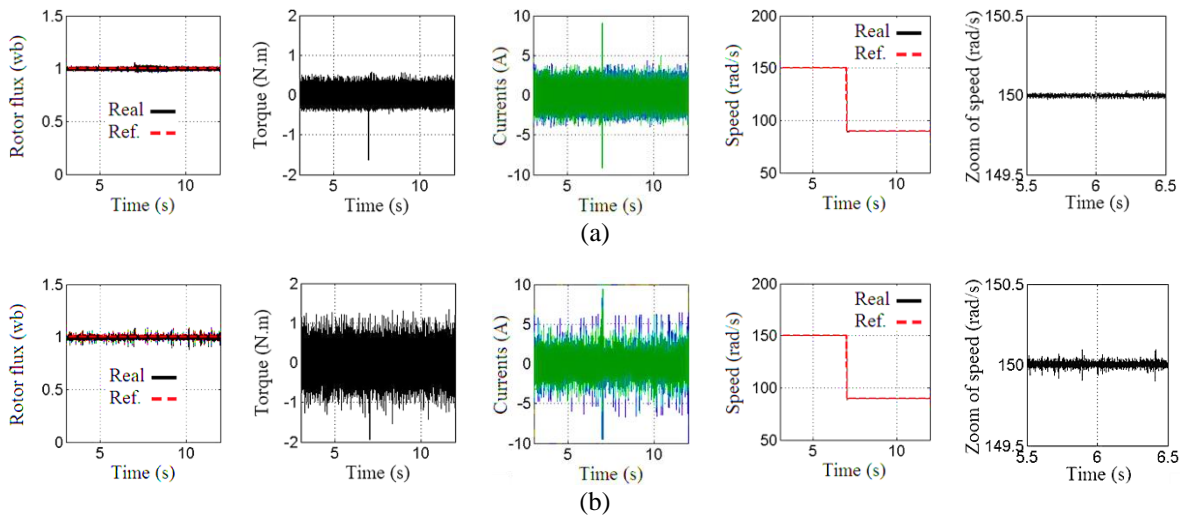


Figure 4. Simulation results of the comparison between the proposed IRFOC method and the conventional IRFOC method for the YCTPIM drive during IGBT-SCF: (a) proposed IRFOC method and (b) conventional IRFOC method

In the second simulation, SSSA is carried out on the YCTPIM during IGBT-SCF under no-load and load conditions. The system matrix (A) is considered, and the eigen values are obtained at each steady-state operating condition. Figure 5 shows the variation of the Eigen values for the faulty drive system over the whole range of speeds. The maximum permissible load is shown in Figure 5(a), $\tau_l = 0 N.m$ and Figure 5(b), $\tau_l = 1.9 N.m$ (maximum permissible load during two-phase mode). The expanded view of Figure 5 that is close to the imaginary axis is also illustrated in this figure. As shown in Figure 5, all eigenvalues have negative real parts, and hence the presented system is asymptotically stable. As shown, the stability analysis has been carried out at different rotor speeds and under no-load and load conditions. The SSSA has been completed based on these operating conditions. It can be mentioned that variations of the motor parameters, a particular value of the mechanical load, and harmonics may lead to instability of the drive system.

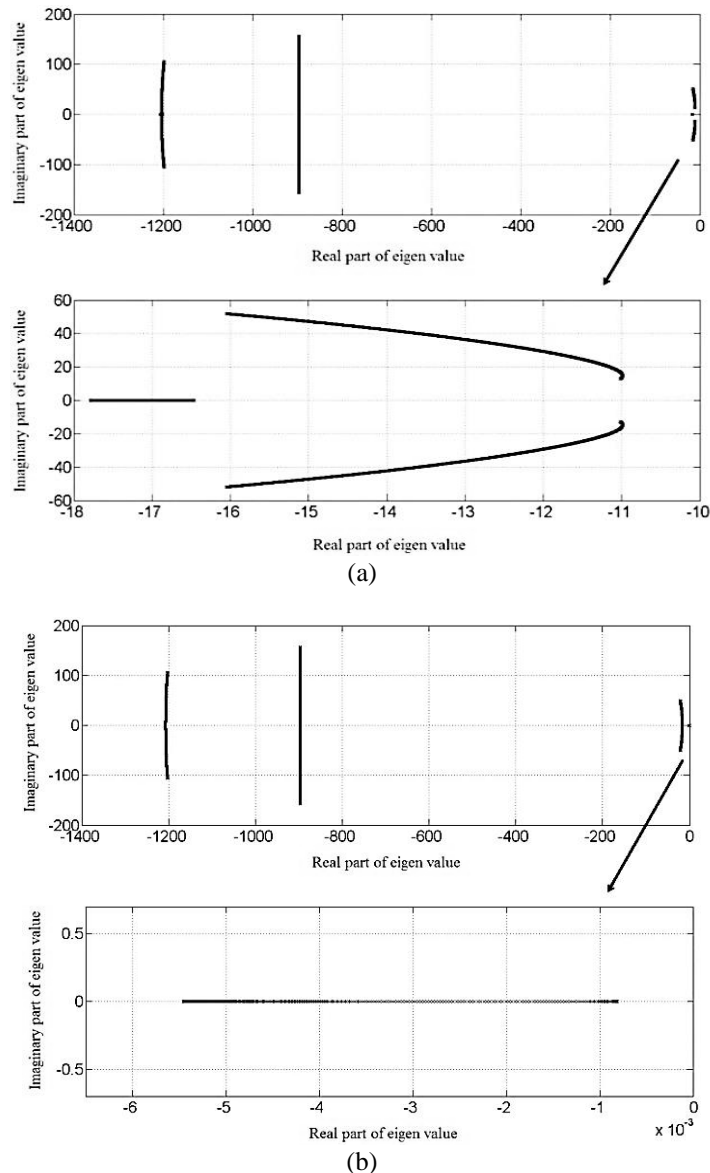


Figure 5. Locus of the eigen values for the faulty drive system over the whole range of speed:
(a) $\tau_l = 0 \text{ N.m}$ and (b) $\tau_l = 1.9 \text{ N.m}$

5. CONCLUSION

In this study, the SSSA of vector-controlled YCTPIM drives during IGBT-SCF is analyzed and discussed. An IRFOC system that operates during IGBT-SCF and is based on a current controller for YCTPIM drives is initially shown. Following this step, the dynamic voltage-current model of the two-phase motor is linearized, and the state-space model that corresponds to it is obtained. After that, the linearized version of the model is utilized so that the system matrix may be obtained. This matrix is utilized in the investigation of the system's stability by means of root locus contours. The SSSA has been carried out at a variety of speeds, taking into consideration both no-load and load scenarios. Simulation research is carried out with the help of MATLAB code. The small-signal model of the system that has been provided can be improved as a future study by taking into consideration the impacts of inverter dead time, harmonics, motor parameter fluctuations, a specific value of the load, and other factors like these.




REFERENCES

- [1] V. L. Kodkin, A. S. Anikin, and A. A. Baldenkov, "Structural correction of nonlinear dynamics of frequency-controlled induction motor drives," *International Journal of Power Electronics and Drive Systems*, vol. 11, no. 1, pp. 220–227, Mar. 2020, doi:




- 10.11591/ijpeds.v11.i1.pp220-227.
- [2] C.-C. Yeh and N. A. O. Demerdash, "Fault-tolerant soft starter control of induction motors with reduced transient torque pulsations," *IEEE Transactions on Energy Conversion*, vol. 24, no. 4, pp. 848–859, Dec. 2009, doi: 10.1109/TEC.2009.2025340.
 - [3] Y. Yu, Y. Zhao, B. Wang, X. Huang, and D. Xu, "Current sensor fault diagnosis and tolerant control for VSI-based induction motor drives," *IEEE Transactions on Power Electronics*, vol. 33, no. 5, pp. 4238–4248, May 2018, doi: 10.1109/TPEL.2017.2713482.
 - [4] V. F. Pires, D. Foito, and J. F. Silva, "Fault-tolerant multilevel topology based on three-phase H-bridge inverters for open-end winding induction motor drives," *IEEE Transactions on Energy Conversion*, vol. 32, no. 3, pp. 895–902, Sep. 2017, doi: 10.1109/TEC.2017.2693563.
 - [5] B. Gou, X. Ge, Y. Liu, and X. Feng, "Load-current-based current sensor fault diagnosis and tolerant control scheme for traction inverters," *Electronics Letters*, vol. 52, no. 20, pp. 1717–1719, Sep. 2016, doi: 10.1049/el.2016.0675.
 - [6] B. Tabbache, M. Benbouzid, A. Kheloui, J.-M. Bourgeot, and A. Mamoune, "An improved fault-tolerant control scheme for PWM inverter-fed induction motor-based EVs," *ISA Transactions*, vol. 52, no. 6, pp. 862–869, Nov. 2013, doi: 10.1016/j.isatra.2013.07.004.
 - [7] R. V. Nemade, J. K. Pandit, and M. V. Aware, "Reconfiguration of T-type inverter for direct torque controlled induction motor drives under open-switch faults," *IEEE Transactions on Industry Applications*, vol. 53, no. 3, pp. 2936–2947, May 2017, doi: 10.1109/TIA.2016.2628721.
 - [8] N. Bianchi, S. Bolognani, M. Zigliotto, and M. Zordan, "Innovative remedial strategies for inverter faults in IPM synchronous motor drives," *IEEE Transactions on Energy Conversion*, vol. 18, no. 2, pp. 306–314, Jun. 2003, doi: 10.1109/TEC.2002.808334.
 - [9] T.-H. Liu, J.-R. Fu, and T. A. Lipo, "A strategy for improving reliability of field-oriented controlled induction motor drives," *IEEE Transactions on Industry Applications*, vol. 29, no. 5, pp. 910–918, 1993, doi: 10.1109/28.245714.
 - [10] R. Maamouri, M. Trabelsi, M. Boussak, and F. M'Sahli, "Fault diagnosis and fault tolerant control of a three-phase VSI supplying sensorless speed controlled induction motor drive," *Electric Power Components and Systems*, vol. 46, no. 19–20, pp. 2159–2173, Dec. 2018, doi: 10.1080/15325008.2018.1534899.
 - [11] Y. Song and B. Wang, "Analysis and experimental verification of a fault-tolerant HEV powertrain," *IEEE Transactions on Power Electronics*, vol. 28, no. 12, pp. 5854–5864, Dec. 2013, doi: 10.1109/TPEL.2013.2245513.
 - [12] D. Kastha and B. K. Bose, "Fault mode single-phase operation of a variable frequency induction motor drive and improvement of pulsating torque characteristics," *IEEE Transactions on Industrial Electronics*, vol. 41, no. 4, pp. 426–433, 1994, doi: 10.1109/41.303793.
 - [13] M. Jannati and N. R. Nik Idris, "Vector control of unbalanced 3-phase IM using forward and backward components," *Turkish Journal of Electrical Engineering & Computer Sciences*, vol. 25, pp. 1358–1374, 2017, doi: 10.3906/elk-1404-545.
 - [14] M. Tousizadeh, H. S. Che, J. Selvaraj, N. A. Rahim, and B.-T. Ooi, "Fault-tolerant field-oriented control of three-phase induction motor based on unified feedforward method," *IEEE Transactions on Power Electronics*, vol. 34, no. 8, pp. 7172–7183, Aug. 2019, doi: 10.1109/TPEL.2018.2884759.
 - [15] M. Jannati, A. Monadi, N. R. N. Idris, and M. J. Abdul Aziz, "Experimental evaluation of FOC of 3-phase IM under open-phase fault," *International Journal of Electronics*, vol. 104, no. 10, pp. 1675–1688, Oct. 2017, doi: 10.1080/00207217.2017.1321144.
 - [16] M. Jannati, N. R. N. Idris, and Z. Salam, "A new method for modeling and vector control of unbalanced induction motors," in *2012 IEEE Energy Conversion Congress and Exposition (ECCE)*, Sep. 2012, pp. 3625–3632, doi: 10.1109/ECCE.2012.6342483.
 - [17] M. Jannati, N. R. N. Idris, and M. J. A. Aziz, "Indirect rotor field-oriented control of fault-tolerant drive system for three-phase induction motor with rotor resistance estimation using EKF," *TELKOMNIKA Indonesian Journal of Electrical Engineering*, vol. 12, no. 9, pp. 6633–6643, 2014.
 - [18] M. Nikpayam, M. Ghanbari, A. Esmaeli, and M. Jannati, "Fault-tolerant control of Y-connected three-phase induction motor drives without speed measurement," *Measurement*, vol. 149, p. 106993, Jan. 2020, doi: 10.1016/j.measurement.2019.106993.
 - [19] T. A. Lipo and E. P. Cornell, "State-variable steady-state analysis of a controlled current induction motor drive," *IEEE Transactions on Industry Applications*, vol. IA-11, no. 6, pp. 704–712, Nov. 1975, doi: 10.1109/TIA.1975.349358.
 - [20] T. Lipo and P. Krause, "Stability analysis of a rectifier-inverter induction motor drive," *IEEE Transactions on Power Apparatus and Systems*, vol. PAS-88, no. 1, pp. 55–66, Jan. 1969, doi: 10.1109/TPAS.1969.292338.
 - [21] E. P. Cornell and T. A. Lipo, "Modeling and design of controlled current induction motor drive systems," *IEEE Transactions on Industry Applications*, vol. IA-13, no. 4, pp. 321–330, Jul. 1977, doi: 10.1109/TIA.1977.4503414.
 - [22] S. Islam, F. I. Bakhsh, S. Ahmad, and A. Iqbal, "Simplified stability analysis of a three-phase induction motor drive system," in *2012 IEEE 5th India International Conference on Power Electronics (IICPE)*, Dec. 2012, pp. 1–6, doi: 10.1109/IICPE.2012.6450367.
 - [23] A. Guha and G. Narayanan, "Small-signal stability analysis of an open-loop induction motor drive including the effect of inverter deadtime," *IEEE Transactions on Industry Applications*, vol. 52, no. 1, pp. 242–253, Jan. 2016, doi: 10.1109/TIA.2015.2464305.
 - [24] V. T. Ha, N. T. Lam, V. T. Ha, and V. Q. Vinh, "Advanced control structures for induction motors with ideal current loop response using field oriented control," *International Journal of Power Electronics and Drive Systems (IJPEDS)*, vol. 10, no. 4, pp. 1758–1771, 2019, doi: 10.11591/ijpeds.v10.i4.pp1758-1771.
 - [25] H. Ismail, F. Patkar, A. Jidin, A. Z. Jidin, N. A. N. Azlan, and T. Sutikno, "Constant switching frequency and torque ripple minimization of DTC of induction motor drives with three-level NPC inverter," *International Journal of Power Electronics and Drive Systems (IJPEDS)*, vol. 8, no. 3, pp. 1035–1049, 2017, doi: 10.11591/ijpeds.v8i3.pp1035-1049.

BIOGRAPHIES OF AUTHORS






Maryam Naghavi    received her B.S. degree in Electrical Engineering from the Khaje Nasir al-Din Tusi University of Technology, Tehran, Iran, in 2007; and her M.S. degree in Electrical Engineering from the Islamic Azad University, Aliabad Katoul, Iran, in 2014. She is presently working towards her Ph.D. degree in Electrical Engineering at the Islamic Azad University, Gorgan, Iran. Her current research interests include the control of AC drives. She can be contacted at email: m.naghavi@gorganiau.ac.ir.






Mahmood Ghanbari    received his B.S. degree in Electrical Engineering from the University of Semnan, Semnan, Iran, in 1996; his M.S. degree in Electrical Engineering from the University of Mazandaran, Babolsar, Iran, in 1999; and his Ph.D. degree in Electrical Engineering from the Science and Research Branch, Islamic Azad University, Tehran, Iran in 2010. He is currently working as an assistant professor at the Gorgan Branch, Islamic Azad University, Gorgan, Iran His current research interests include the control of AC drive systems and DSP applications in power electronic systems. He can be contacted at email: ghanbari@gorganiau.ac.ir.






Reza Ebrahimi    is currently an assistant professor at the Department of Electrical Engineering in Gorgan Branch of Islamic Azad University. His research interests include network integration of distributed energy resource and distribution system analysis. He can be contacted at email: R.ebrahimi@gorganiau.ac.ir.



Mohammad Jannati    received his B.S. degree in Electrical Engineering from the University of Mazandaran, Babolsar, Iran, in 2008; his M.S. degree in Electrical Engineering from the University of Guilan, Rasht, Iran, in 2010; and his Ph.D. degree in Electrical Engineering from the Universiti Teknologi Malaysia (UTM), Kuala Lumpur, Malaysia in 2014. He is currently working as a Lecturer at the Islamic Azad University, Gorgan, Iran. His current research interests include the control of AC drive systems and DSP applications in power electronic systems. He can be contacted at email: M.Jannati@gorganiau.ac.ir.



Tole Sutikno    is a lecturer in Electrical Engineering Department at the Universitas Ahmad Dahlan (UAD), Yogyakarta, Indonesia. He received his B.Eng., M.Eng. and Ph.D. degrees in Electrical Engineering from Universitas Diponegoro, Universitas Gadjah Mada, and Universiti Teknologi Malaysia, in 1999, 2004 and 2016, respectively. He has been an Associate Professor in UAD, Yogyakarta, Indonesia since 2008. He is currently an Editor-in-Chief of the TELKOMNIKA and the Head of the Embedded Systems and Power Electronics Research Group (ESPERG). His research interests include the field of digital design, industrial applications, industrial electronics, industrial informatics, power electronics, motor drives, renewable energy, FPGA applications, embedded system, artificial intelligence, intelligent control, information technology and digital library. He can be contacted at email: tole@te.uad.ac.id, tole@ee.uad.ac.id.